Electronic Journal of Biotechnology 79 (2026) 100698

Contents lists available at ScienceDirect

Electronic Journal of Biotechnology

journal homepage: www.elsevier.com/locate/ejbt

Research article

Biogenic synthesis of silver nanoparticles using cell-free extracts of thermotolerant bacteria: Antioxidant and antibacterial properties ☆

Aparna Banerjee [a,1,*], Ismael Herrera-Vargas [b,1], Mario E. Flores [c], Francisca Valenzuela [a], Srijan Banerjee [d]

[a] Functional Polysaccharides Research Group, Instituto de Ciencias Aplicadas, Facultad de Ingeniería, Universidad Autónoma de Chile, Talca, Chile
[b] Escuela de Ingeniería en Biotecnología, Facultad de Ciencias Agrarias y Forestales, Universidad Católica del Maule, Talca, Chile
[c] Instituto de Ciencias Químicas, Facultad de Ciencias, Isla Teja, Universidad Austral de Chile, Valdivia 5090000, Chile
[d] PhD Program in Science, R&D Bioactive Products Department, Chemistry Institute of Natural Resources, Universidad de Talca, Talca, Chile

GRAPHICAL ABSTRACT

Biogenic synthesis of silver nanoparticles using cell-free extracts of thermotolerant bacteria: Antioxidant and antibacterial properties

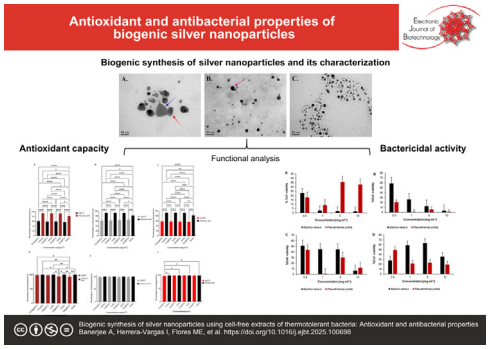

ARTICLE INFO

Article history:
Received 12 June 2025
Accepted 26 August 2025
Available online 23 November 2025

Keywords:
Antibacterial
Antioxidant
Bacillus haynesii
Biogenic synthesis
Biosynthesized nanoparticles
Cell-free extracts
Pseudomonas alcaligenes
Silver nanoparticles
Staphylococcus sp.
Thermotolerant bacteria

ABSTRACT

Background: Eco-friendly synthesis of silver nanoparticles (AgNPs) using biological systems offers a sustainable alternative to conventional physicochemical methods. In this study, we employed cell-free extracts from three thermotolerant bacterial strains, *Bacillus haynesii* CamB6, *Pseudomonas alcaligenes* Med1, and *Staphylococcus* sp. BSP3 for the biosynthesis of AgNPs, aiming to explore their antioxidant and antibacterial properties.

Results: The biosynthesized AgNPs were characterized through UV–Vis spectroscopy, FTIR, TEM, and DLS analyses, which revealed distinct physicochemical profiles among the nanoparticles. Notably, AgNP2 and AgNP3 exhibited smaller particle sizes, enhanced colloidal stability, and superior biological activities compared to AgNP1. Antioxidant evaluation demonstrated significant free radical scavenging potential, with AgNP2 showing the highest DPPH activity (65.18% at 5 mg mL^{-1}). Antibacterial activity, assessed via agar well diffusion and cell viability assays against *Bacillus cereus* and *Pseudomonas putida* revealed that AgNP2 achieved the lowest bacterial viability (0.74%) for *P. putida* at 1 mg mL^{-1} concentration.

Conclusions: The study highlights the potential of biosynthesized AgNPs, particularly AgNP2, as sustainable for biomedical applications. Their antioxidant and antibacterial activities suggest valuable applications in managing oxidative stress and combating antimicrobial resistance.

☆ Audio abstract available in Supplementary material.

Peer review under responsibility of Pontificia Universidad Católica de Valparaíso.

* Corresponding author.
E-mail address: aparna.banerjee@uautonoma.cl (A. Banerjee).

[1] Both are equally first authors.

https://doi.org/10.1016/j.ejbt.2025.100698

How to cite: Banerjee A, Herrera-Vargas I, Flores ME, et al. Biogenic synthesis of silver nanoparticles using cell-free extracts of thermotolerant bacteria: Antioxidant and antibacterial properties. Electron J Biotechnol 2026:79. https://doi.org/10.1016/j.ejbt.2025.100698.

1. Introduction

Nanotechnology has transformed numerous scientific disciplines with significant improvements in healthcare [1], environmental sciences [2,3,4], and material engineering. Among the various nanoparticles [5,6,7], silver nanoparticles (AgNPs) stand out for their unique physicochemical properties, including antimicrobial, antioxidant, and catalytic activities [8,9]. These properties make AgNPs indispensable in biomedical applications, such as drug delivery systems, wound dressings, biosensors, and potential weapons in combating antimicrobial resistance [10,11]. The traditional synthesis of AgNPs often involves energy-intensive physical and chemical methods that generate hazardous by-products, posing environmental concerns. As an alternative, green synthesis methods employing biological systems such as plants, fungi, and bacteria have gained attention [12]. These methods are cost-effective and environmentally sustainable, leveraging natural reducing agents to produce nanoparticles with enhanced biocompatibility [13,14]. Despite growing interest in biosynthesized AgNPs, limited studies have systematically compared the influence of thermotolerant bacterial extracts on nanoparticle stability and biological function. Most prior work has focused on plant- or mesophilic bacteria-derived nanoparticles, often without detailed physicochemical-biological correlation. This study addresses this gap by employing thermotolerant strains with known bioactive compound production to explore the strain-specific impact on AgNP morphology, stability, and activity. Among the biological sources, thermotolerant bacteria are particularly advantageous due to their ability to thrive under extreme environmental conditions, making their metabolic products stable and efficient in nanoparticle synthesis [15,16].

AgNPs synthesized through green methods have demonstrated significant antioxidant potential by scavenging reactive oxygen species (ROS) and inhibiting oxidative stress pathways [9,17]. This property addresses oxidative stress-related diseases like neurodegenerative disorders, cardiovascular diseases, and cancer. Additionally, the antioxidant properties of AgNPs enhance their stability, reducing aggregation and maintaining their functional integrity in biomedical applications [8,18]. Additionally, the rising threat of antimicrobial resistance (AMR) underscores the need for novel therapeutic strategies. AgNPs exhibit broad-spectrum antimicrobial activity by disrupting bacterial membranes, denaturing proteins, and generating ROS, leading to bacterial cell death [19,20]. These mechanisms make AgNPs effective against gram-positive and gram-negative bacteria [21], including multidrug-resistant strains [11,22]. Furthermore, the integration of AgNPs in combination therapies has shown promise in enhancing the efficacy of traditional antibiotics while mitigating resistance development [23,24]. Our group has previously demonstrated similar applications of biopolymer-mediated nanoparticle synthesis for biomedical and environmental uses [12,25,26].

In the present study, we focused on the biosynthesis of AgNPs using cell-free extracts from thermotolerant bacterial strains *Bacillus haynesii* CamB6 [27], *Pseudomonas alcaligenes* Med1 [28], and *Staphylococcus* sp. BSP3 [29]. These bacteria were chosen for their ability to produce thermostable compounds with robust enzymatic systems and peptide or exopolysaccharide production. These bioactive compounds can retain their functionality at elevated temperatures (≥55°C). In the cell-free extracts, these biopolymers can efficiently reduce Ag^+ ions to Ag^0 and simultaneously also help in capping the formed nanoparticles that promote colloidal stability enhancement without the need for chemical additives [25,27,28,30,31]. In previous report by Nas et al. [32] revealed key secondary metabolites of crude extracts from halotolerant *Bacillus* sp. such as Hexadecanoic acid, 2,4-Di-*tert*-butyl-phenol, 2,4,6-Tri-*tert*-butylphenol, 3,5-Di-*tert*-butyl-4-hydroxybenzaldehyde, 7-Acetyl-6-ethyl-1,1,4,4-tetramethyl-1,2,3,4-tetrahydronaphthalene, etc. Phenolic compounds are widely known as reducing and stabilizing agents in green AgNP synthesis. Previously, dihydroxybenzene derivatives have been experimentally demonstrated to reduce Ag^+ to Ag^0 and form stable AgNPs through electron transfer pathways [33]. Furthermore, n-hexadecanoic acid (palmitic acid), oleic acid, and other long-chain fatty acids have been identified as effective capping agents, enhancing colloidal stability and preventing particle aggregation in biofabricated AgNPs [34]. Recently, Ashrafi-Saiedlou et al. [35] reported a similar set of metabolites, such as alcoholic, phenolic or amino compounds, present in the bacterial cell-free supernatant of *Pseudomonas fluorescens* that also contribute to the reduction and stabilization of nanoparticles by promoting electrostatic interactions and hydrogen bond formation with nanoparticle surfaces. In 2022, Fedorova et al. [36] reported cell-free supernatant of *Staphylococcus aureus* culture is abundant with antimicrobial peptides. These antimicrobial peptides often contain multiple cysteine residues that form disulfide bridges (–S–S–) which stabilizes the peptide's 3D structure. Thiol (–SH) groups can also donate electrons to silver ions (Ag^+) which can reduce them to metallic silver (Ag^0) [37]. Furthermore, thermotolerant strains offer a more robust, cleaner, and reproducible green synthesis platform for AgNPs with desirable physicochemical and biological properties as conducting the synthesis and bacterial culture under elevated temperature helps suppress the growth of unwanted mesophilic contaminants [38]. The biosynthesized AgNPs were characterized by their size, morphology, and surface charge. Their biological activities, including antibacterial and antioxidant properties, were systematically evaluated to explore their potential in addressing antibacterial potential and oxidative stress-related challenges. By utilizing green synthesis methods using bacterial cell-free supernatants, this study aims to provide a sustainable and effective approach to AgNP production, with implications for their application in biotechnology, nanobiomedicine and beyond. The results highlight the potential of biosynthesized AgNPs as a versatile platform for developing next-generation biomedical solutions.

2. Materials and methods

2.1. Bacterial strains and culture conditions

Three thermotolerant bacterial strains *B. haynesii* CamB6, *Pseudomonas alcaligenes* Med, and *Staphylococcus* sp. BSP3, which were selected for the biosynthesis of AgNPs, were previously isolated by our research group from hot spring environments in the Maule

region of Chile, such as Campanario (35°56′23″ S 70°36′22″ W), Medano (35°57′33″S 70°77′85″W) and San Pedro hot spring (35°08′ 12″ S, 70°28′ 36″ W), respectively. These strains were cultivated in nutrient broth (NB, HiMedia, India) at their optimal growth temperatures 37°C for *P. alcaligenes* and *Staphylococcus* sp., and 50°C for *B. haynesii*) as previously reported [27,28,29]. Cultures were maintained under aerobic conditions, under continuous agitation at 150 rpm for 24 h.

2.2. Preparation of bacterial cell-free extracts

After the incubation period to obtain stationary phase growth, the bacterial cultures were centrifuged (Orto Alresa SKU ECE110, Spain) at 5000 rpm for 15 min at 4°C to separate the cells. Then, the supernatants were filtered through a 0.22 μm membrane filter to ensure the removal of residual cells and debris, as mentioned previously by Focardi et al. [39]. The resulting cell-free extracts were stored at 4°C until further use in nanoparticle synthesis.

2.3. Biogenic synthesis of AgNPs

Bacterial cell-free extracts as substrate and silver nitrate ($AgNO_3$, HiMedia, India) as precursor were used to biosynthesize the AgNPs. For this, a 10 mM $AgNO_3$ aqueous solution was prepared and added to the bacterial cell-free extracts in 1:1 (v/v) under sterile conditions. Each reaction mixture was prepared separately and incubated at 30°C (Labwit ZWY – 2102C, Australia) in the dark with continuous shaking at 150 rpm for 48 h. The synthesis of AgNPs was monitored by observing a color change from pale yellow to brown, indicating nanoparticle formation. These AgNPs were used to evaluate the effect of silver ion concentration and stability. Further, the colloidal AgNP suspension was centrifuged (8000 rpm, 15 min, 4°C), washed, and lyophilized for further usage.

2.4. Characterization of AgNPs

2.4.1. Spectroscopic analysis

The formation of AgNPs was confirmed using a UV–vis spectrophotometer (Shimadzu UV-1800, Japan) by scanning the reaction mixture in the wavelength range of 300–500 nm. The characteristic surface plasmon resonance (SPR) peak of AgNPs was observed, indicating successful nanoparticle synthesis. A baseline correction was performed using distilled water as a reference to ensure accuracy. All the studies were performed in triplicates. The Fourier Transform Infrared (FTIR) spectra of the biosynthesized AgNPs were obtained using a Jasco spectrometer (FT-IR 4600) equipped with an ATR accessory (ATR 550 S, Jasco) for enhanced surface sensitivity. A 100 μL aliquot of the colloidal AgNPs suspension was carefully deposited onto the ATR crystal, ensuring even coverage for accurate analysis. The spectra were recorded over a wavenumber range of 400–4000 cm^{-1}.

2.4.2. Transmission electron microscopic (TEM) analysis

The size and morphology of the synthesized AgNPs were analyzed using Transmission Electron Microscopy (TEM) (JEOL JSM 1200EX-II, Japan). For this, the lyophilized AgNPs were resuspended in distilled water to prepare a suspension. One drop of this suspension was placed on a copper electron microscope grid pre-coated with a carbon film, air-dried overnight and observed. High-resolution images were captured to assess the particle size distribution, shape uniformity, and surface morphology of the AgNPs. The mean sizes were calculated from multiple fields of view. All the studies were performed in triplicates.

2.4.3. Dynamic light scattering (DLS)

The particle size distribution, polydispersity index (PDI), and zeta potential of the synthesized AgNPs were measured using a DLS analyzer (Malvern Zetasizer Nano ZS, UK) with backscattering detection (173°). Measurements were conducted at 25°C with a scattering angle of 173° using disposable cuvettes for particle size and zeta potential analysis (DTS1070, Malvern, UK). Each sample was measured in triplicate, and the average values with standard deviations were reported to ensure reproducibility and accuracy.

2.5. Antioxidant activity of the AgNPs

2.5.1. DPPH radical scavenging activity

The radical scavenging activity (RSA) of 2,2-diphenyl-1-picrylhydrazyl (DPPH) was determined following the methods given by Shimada et al. [40] with some modifications. In summary, different concentrations of 200 μL of NPs aqueous solution (0.5, 1, 2, and 5 mg mL^{-1}) were mixed with 20 μL (0.2 mM) ethanolic DPPH solution. The mixture was then kept in the dark at 30°C for 1 h and subsequently centrifuged at 5000 rpm for 10 min. The absorbance of the supernatant was measured at 517 nm using a microplate reader (Allsheng, Flex A-200, China). [Equation 1] was used to calculate the DPPH scavenging activity:

$$\left[\frac{(A-B)}{A}\right] \times 100 \quad (1)$$

where A is the absorbance of the control supernatant and B is the absorbance of the sample, respectively.

2.5.2. Hydrogen peroxide scavenging activity

The H_2O_2 scavenging activity of the AgNPs was assessed using a modified version of the method described by Ruch et al. [41]. In a 96-well microplate, 50 μL of AgNP sample was mixed with 120 μL of phosphate buffer (0.1 mM, pH 7.4) and 30 μL of H_2O_2 solution. The mixture was incubated at 30°C in the dark for 10 min. Positive and negative controls were prepared using 100 μL of 10 mM $AgNO_3$ aqueous solution and 100 μL of NB medium, respectively. Additionally, samples without H_2O_2 were used to measure baseline absorbance. After incubation, absorbance was measured at approximately 230 nm using a UV–Vis microplate reader (Allsheng, FlexA-200, China). The antioxidant activity was calculated using the following formula [Equation 2]:

$$\left[1-\frac{(A1-A2)}{A0}\right] \times 100 \quad (2)$$

where A_0 is the absorbance of the control, A_1 is the absorbance of the reaction sample, and A_2 is the sample without H_2O_2.

2.6. Antibacterial activity of the AgNPs

2.6.1. Agar well diffusion assay

For the qualitative agar well diffusion assay, according to Chavez-Esquivel et al. [42], with a little modification, gram-negative *Pseudomonas putida* (ATCC 12633) and gram-positive *Bacillus cereus* (ATCC 14579) cultures were used. Mueller-Hinton agar (MH, HiMedia, India) plates were prepared, and each plate was inoculated with 100 μL of fresh bacterial suspension (OD_{590} = 0.1, corresponding to approximately 1×10^8 CFU mL^{-1} cells) evenly spread using a sterile L-shaped spreader. Once the inoculum dried, wells in triplicate were created in the agar using a sterile cork borer. Control plates were prepared without agar well. AgNP samples were added to the wells at volumes of 100 μL, 200 μL, and 300 μL, respectively. A 20 μL of the third-generation cephalosporin antibiotic Cefotaxime was used as a positive control because of its broad-spectrum activity against both

Gram-negative and some Gram-positive bacteria. 20 μL $AgNO_3$ which is the precursor salt of AgNPs was used as a negative control to distinguish the effect of ionic silver from that of the nanoparticulate form. The procedure was repeated in triplicates. The plates were sealed and incubated (BJPX-Wichita, China) at 30°C for 16 h. Growth inhibition was determined by measuring the halo diameter around the wells.

2.6.2. Bacterial cell viability assay

For quantitative expression of the antibacterial property of the biosynthesized AgNPs, the viability of the studied gram-positive and gram-negative bacterial cells treated with AgNPs was evaluated. Fresh overnight stationary phase (~1 × 10^8 CFU mL^{-1}) *P. putida* and *B. cereus* cultures were prepared in NB medium. Sterilized Falcon tubes (50 mL) were filled with 10 mL of autoclaved LB medium, to which 500 μL of each bacterial suspension was added. AgNPs were added to the tubes at four final concentrations: 0.5 mg mL^{-1}, 1 mg mL^{-1}, 5 mg mL^{-1}, and 10 mg mL^{-1}. Each concentration was tested in triplicate for both bacterial strains alongside the positive and negative controls. The treatments were incubated at 30°C, 150 rpm, shaking in a BJPX-Wichita incubator (Biobase, China) for 24 h. The viability of the bacterial cells was observed *via* staining with LIVE/DEAD™ BacLight™ (Thermo Fisher Scientific, USA). SYTO 9 green stains live cells in a fresh sample, whereas propidium iodide (PI) red only stains dead cells and extracellular DNA (eDNA). The stained cells were observed with a Leica Stellaris 5 confocal microscope (Leica Microsystems, Germany) with excitation/emission for SYTO 9 of 485 nm/498 nm and PI of 535 nm/617 nm. Quantifying live and dead cells was performed using ImageJ software [43], and the results were expressed as a percentage of viable bacteria relative to untreated controls.

2.7. Statistical analysis

Graphpad Prism version 9.5, Biorender and OriginPro 2018 have been used for graphical representations. All of the studies were performed in replicates, and all data were represented with mean ± SD. Graphpad Prism version 9.5 was utilized to perform pairwise comparison of DPPH and H_2O_2 scavenging activity in each concentration of AgNPs and ascorbic acid through one-way ANOVA with Šídák's multiple comparisons test, where the threshold significance level was 0.05. Heteroscedasticity was checked using the Brown-Forsythe test.

3. Results and discussion

3.1. Characterization of AgNPs

3.1.1. Spectroscopic analysis

The formation of biosynthesized AgNPs was confirmed using UV–vis spectroscopy, a standard technique for analyzing the optical properties of nanoparticles. The spectra were recorded in the 300–500 nm wavelength range using a UV–vis microplate reader (FlexA-200, China). All three AgNP samples exhibited a characteristic surface plasmon resonance (SPR) peak centered around 450 nm (Fig. S1). This is indicative of the successful formation of AgNPs, as previously reported. The appearance of absorption peaks in this region corresponds to the wavelength of the SPR phenomenon, confirming nanoparticle synthesis [44,45]. Interestingly, variations in the intensity of the SPR peaks were observed among the AgNPs synthesized by the cell-free supernatant of three different bacterial strains. The SPR peak intensity for *Staphylococcus* sp. BSP3 AgNP3 was the highest, followed by *P. alcaligenes* Med1 AgNP2, and the lowest intensity was observed for *B. haynesii* CamB6 AgNP1. This difference in peak intensity suggests variability in the nanoparticle concentration, size distribution, or stabilization efficiency among the bacterial strains, as previously reported in studies examining the influence of these factors on the surface plasmon resonance properties of AgNPs [3,22]. The absorbance values near the SPR peaks were nearly around 0.8 A.U. Similar absorbance values of SPR peaks were observed in a previous report by Gusrizal et al. [46], where AgNPs were produced by the reduction of $AgNO_3$ with m-hydroxybenzoic acid. Nevertheless, they reported the intensity of similar SPR peaks at 66 and 50 times lesser concentrations of $AgNO_3$ where they have used m-hydroxybenzoic acid in pH 11 at 1.0×10^{-3} M and 1.0×10^{-2} M concentrations, respectively. That may be due to the lower availability of silver ions (Ag^+) in the culture media, as these ions were reported to form complexes with chloride (Cl^-) and phosphate (PO_4^{3-}) ions in the media. Silver entrapped in those highly insoluble (pKS = 9.8) complexes also exhibits a very limited ability to bind with bacterial membranes and cell walls [47,48]. Furthermore, Hydroxybenzoic acid, particularly 4-hydroxybenzoic acid (4-HBA), is naturally produced by some bacteria through the shikimate pathway, which functions as a crucial metabolic route for the synthesis of aromatic amino acids like phenylalanine, tyrosine, and tryptophan by converting phosphoenolpyruvate (PEP) and erythrose 4-phosphate into chorismate [49,50]. The color change of the reaction mixtures from pale yellow to reddish-brown further validated the reduction of Ag^+ to elemental silver (Ag^0). Control samples lacking nanoparticles did not exhibit any SPR peaks, confirming that the absorption peaks observed were explicitly due to the biosynthesized AgNPs.

FTIR spectroscopy of the biosynthesized silver nanoparticles (AgNP1, AgNP2, and AgNP3) revealed distinct functional groups of the bacterial cell-free supernatant, possibly involved in the reduction, stabilization, and capping processes (Fig. 1). The presence of hydroxyl, amide, polysaccharide, and other biomolecular groups from the bacterial supernatants provided insight into the role of bacterial strain characteristics in determining the stability and properties of the nanoparticles. In the case of AgNPs, the O—H/N—H stretching at ~3410–3420 cm^{-1} is due to the hydroxyl and amine groups indicative of alcohols, phenols, and proteins. Hydroxyl groups have been reported to play a crucial role earlier in reducing silver ions and stabilizing nanoparticles [9,11,22]. The C═O stretching at ~1630–1640 cm^{-1} probably indicates the carbonyl groups from proteins or amides acting as capping agents, as previously reported by Karthik et al. [51] and Sidhu et al. [52]. The C—O stretching around ~1060–1100 cm^{-1} is the presence of possible polysaccharides, represented by C—O stretching vibrations, which are known to form steric barriers around nanoparticles [9]. For AgNP2, the C—H/N—O bending around ~1380 cm^{-1} can be due to the secondary metabolites or nitrates enhancing nanoparticle stability, as reported by Ravindran et al. [13]. Finally, for AgNP3, aromatic/halide deformation around ~620 cm^{-1} indicates unique aromatic or halide groups produced by the bacteria, suggesting bacterial strain-specific biomolecular interactions that enhance green nanoparticle stabilization [22].

These findings highlight the significant role of biomolecules produced by the bacteria, such as hydroxyl, amide, and polysaccharide groups, in the reduction, stabilization, and capping processes during the green synthesis of AgNPs. The observed differences in functional group composition among AgNP1, AgNP2, and AgNP3 emphasize the influence of bacterial strain-specific biochemical profiles on nanoparticle properties, including size, stability, and dispersion. Notably, the unique contributions of aromatic or halide groups in AgNP3 suggest a possible enhanced stabilization mechanism, potentially leading to superior colloidal stability and functionality. This study underscores the potential of tailoring nanoparticle properties by selecting specific bacterial strains and their associated biomolecules, paving the way for advanced appli-

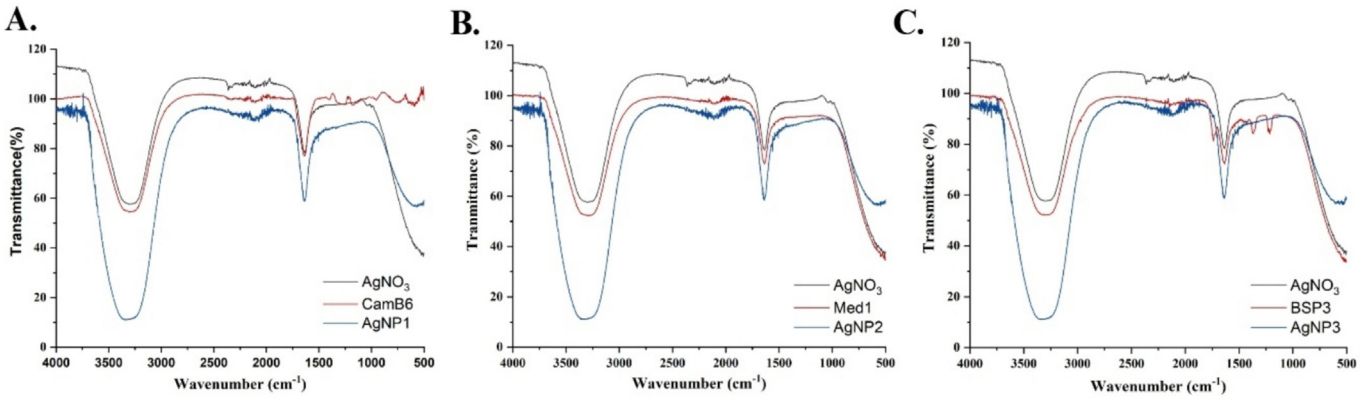

Fig. 1. FTIR spectra showing the biosynthesized AgNP1 (A), AgNP2 (B), and AgNP3 (C) having distinct functional groups than those of the bacterial cell-free supernatant, possibly involved in the reduction, stabilization, and capping processes.

cations in biomedicine, environmental remediation, and nanotechnology.

3.1.2. Transmission electron microscopic (TEM) analysis

The size, morphology, and distribution of the biosynthesized AgNPs were further analyzed using TEM (JEOL JSM 1200EX-II, Japan). The TEM images revealed that the nanoparticles were predominantly spherical with a relatively uniform size distribution (Fig. 2A–C). The average particle sizes were determined based on manually annotated measurements within the TEM images: *Staphylococcus* sp. BSP3 AgNP3: Mean size = 8.40 ± 5.21 nm, *P. alcaligenes* Med1 AgNP2: Mean size = 10.78 ± 6.40 nm, and *B. haynesii* CamB6 AgNP1: Mean size = 20. 82 ± 12.56 nm. The smallest particles were observed in AgNP3 synthesized using the cell-free supernatant of *Staphylococcus* sp. BSP3 also exhibited the highest SPR peak intensity, correlating nanoparticle size with optical properties. In contrast, AgNP1 produced by *B. haynesii* CamB6 showed larger particles, consistent with the lower SPR intensity observed in the UV–Vis analysis.

The TEM images confirmed the relatively monodispersed nature of the nanoparticles, with minimal aggregation observed, indicating effective stabilization by biomolecules present in the bacterial cell-free supernatants. Going into further detail after studying the morphology of the NPs synthesized by cell-free supernatants of different bacteria, it is observable that AgNP1 had spherical particles along with noticeable triangular and rod-like NPs. In the case of AgNP2, nanoparticles were primarily spherical, but occasional irregular shapes were observed. Finally, for AgNP3, NPs were predominantly spherical. It may be highlighted that AgNP3 was synthesized using *Staphylococcus* sp. BSP3 demonstrated the most uniform size distribution and shape, which may account for its higher SPR peak intensity observed in the UV–Vis analysis. Regarding heterogeneity, AgNP1 exhibited the highest variability in shape and size, with spherical, triangular, and rod-like particles observed. A clear and smooth surface morphology suggests a uniform reduction and capping process [13]. These findings highlight the influence of bacterial strain characteristics on the size and morphology of the synthesized AgNPs, which directly impact their physical and biological properties. Previously, Saeed et al. [53] reported biosynthesis of AgNPs from soil-origin *Escherichia coli*, *Exiguobacterium aurantiacum*, and *Brevundimonas diminuta,* where the sizes ranged from 5 to 50 nm, indicating how different bacterial strains may influence the synthesis and characteristics of AgNPs.

3.1.3. Dynamic light scattering (DLS)

The size distribution, polydispersity index (PDI), and zeta potential of the biosynthesized AgNPs were determined using DLS analysis (Malvern Zetasizer Nano ZS, UK). This analysis provided insights into the hydrodynamic diameter and colloidal stability of the nanoparticles [54,55]. The hydrodynamic diameter typically includes the nanoparticle core and the biomolecular capping layer, leading to slightly larger sizes compared to TEM measurement [54,56]. AgNP1 had a hydrodynamic diameter of 56. 73 ± 0.44 nm with a PDI of 0.237 ± 0.003 and a Zeta potential of −37.0 ± 1.4 mV, while the hydrodynamic diameter of AgNP2 is 55.4 ± 2.29 nm with a PDI of 0.50 ± 0.1 and a Zeta potential −43. 3 ± 2.9 mV. Finally, the hydrodynamic diameter of AgNP3 is observed to be 44.43 ± 0.41 nm, along with a PDI of 0.29 ± 0.007 and −26.2 ± 1.4 mV Zeta potential (Fig. 2D–L).

The results indicate that AgNP3 was synthesized using the cell-free extract of *Staphylococcus* sp. BSP3 exhibited the most minor hydrodynamic diameter and the lowest PDI. This shows a more monodispersed and stable nanoparticle suspension, as previously mentioned by Danaei et al. [57]. This is attributed to the diverse functional groups that synergistically provide strong electrostatic and steric stabilization, as may be observed from the FTIR characterization. In contrast, AgNP1 showed the largest hydrodynamic diameter and the highest PDI. This suggests more significant heterogeneity and aggregation potential [57]. The stabilization of AgNP1 may be attributed to electrostatic interactions from carbonyl and hydroxyl groups and steric stabilization by polysaccharides, as observed before from the spectroscopic characterization. However, its larger particle size and higher polydispersity index suggest less efficient stabilization compared to AgNP2 and AgNP3. This may result from lower concentrations or reduced diversity of biomolecules produced by *B. haynesii* CamB6 in its supernatant. AgNP2 displayed intermediate values, reflecting a balance between particle size and stability. This trend was previously observed in the TEM analysis, too, which is further confirmed with the DLS study. The zeta potential values for all samples were negative, confirming the presence of surface charges that contribute to the electrostatic stabilization of the nanoparticles [58]. AgNP2 additionally exhibited the highest negative zeta potential of −43.3 mV, which correlates with its improved colloidal stability and relative monodispersity. These findings also align with the results from TEM analysis, highlighting the influence of bacterial strain characteristics on the colloidal properties of biosynthesized AgNPs. DLS, along with TEM analyses, has already been suggested to be the roadmap for the correct characterization of AgNPs [56], which can be observed in our study, too.

3.2. Antioxidant activity of the AgNPs

3.2.1. DPPH radical scavenging activity

The antioxidant activity of the biosynthesized silver nanoparticles (AgNP1, AgNP2, and AgNP3) was evaluated using the DPPH radical scavenging assay and compared with ascorbic acid as a

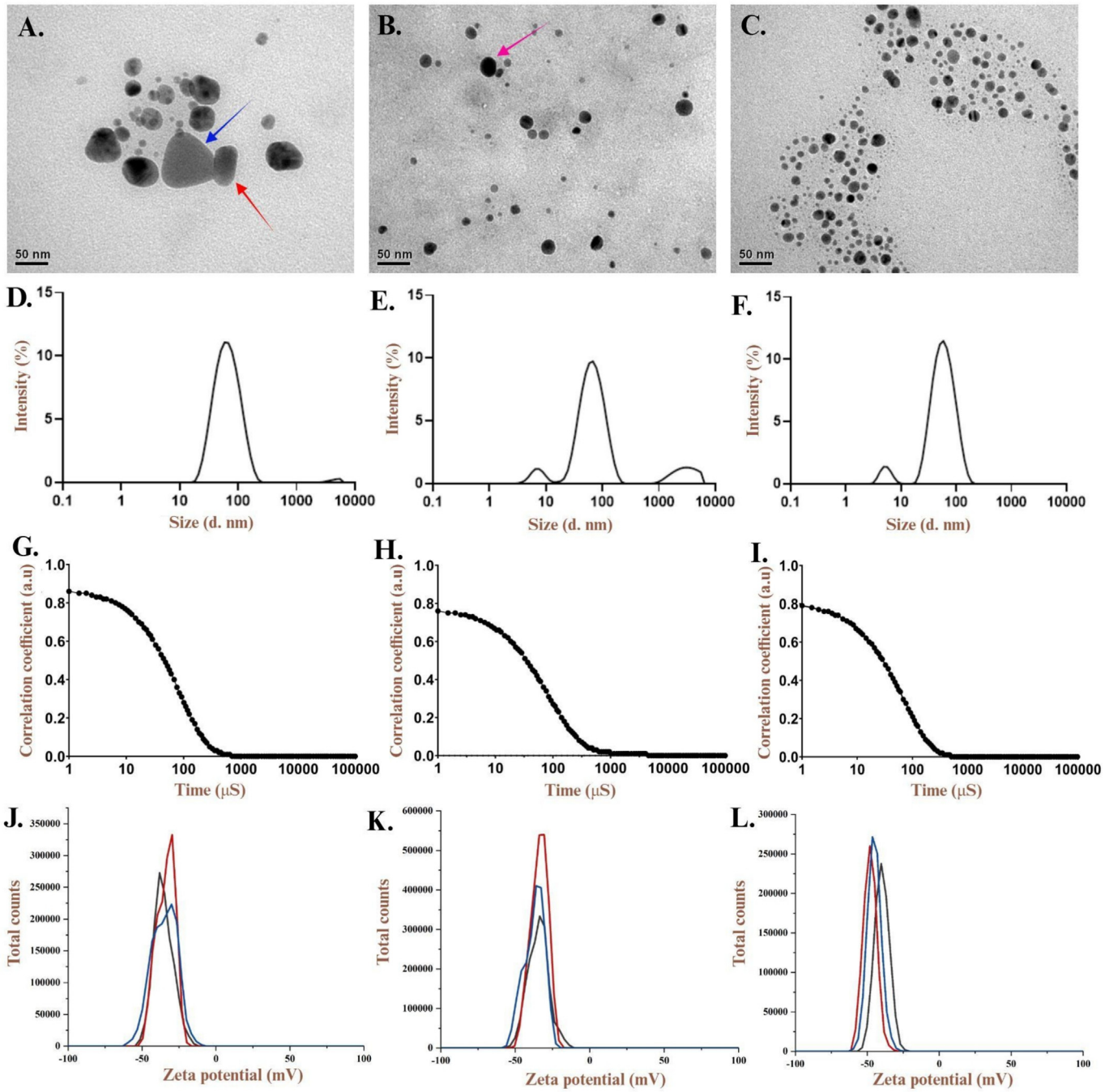

Fig. 2. Characterization of biosynthesized silver nanoparticles (AgNPs) using Transmission Electron Microscopy (TEM), Dynamic Light Scattering (DLS), and Zeta potential analysis. **(A–C)** TEM micrographs of AgNP1 (A), AgNP2 (B), and AgNP3 (C). Nanoparticles are mostly spherical; AgNP1 (A) shows shape heterogeneity with triangular (blue arrow), rod-like (red arrow), and spherical forms, while AgNP2 (B) includes irregular shapes (magenta arrow), and AgNP3 (C) displays highly uniform spherical morphology. Scale bars represent 50 nm. **(D–F)** DLS particle size distribution by intensity for AgNP1 (D), AgNP2 (E), and AgNP3 (F), showing relative hydrodynamic diameter profiles. **(G–I)** Autocorrelation function plots for AgNP1 (G), AgNP2 (H), and AgNP3 (I), representing light scattering decay curves used to derive nanoparticle diffusion coefficients and size. **(J–L)** Zeta potential measurements of AgNP1 (J), AgNP2 (K), and AgNP3 (L), indicating surface charge distributions. Negative zeta potentials reflect electrostatic stability in colloidal suspension. (For interpretation of the references to color in this figure legend, the reader is referred to the web version of this article).

standard antioxidant. The scavenging activity was assessed at 0.5, 1, 2, and 5 mg mL^{-1} concentrations. Among the tested samples, ascorbic acid exhibited the highest DPPH radical scavenging activity across all concentrations (adjusted p-value < 0.0001 for almost all AgNP vs. all tested concentrations of ascorbic acid comparisons), with a maximum activity of 92.89 ± 0.01% at 1 mg mL^{-1} concentration and a slight decrease at 5 mg mL^{-1} (82.5 ± 0.05%). For the AgNPs, the scavenging activity followed the AgNP2 > AgNP1 > AgNP3 trend at all tested concentrations (Fig. 3A–C). At 0.5 mg mL^{-1}, AgNP1 and AgNP2 showed nearly similar scavenging activities of ~60%, while AgNP3 exhibited a lower activity of 49.41 ± 0.19%. A similar pattern was observed at higher concentrations, with AgNP2 reaching its highest activity of 65.18 ± 0.11% at 5 mg mL^{-1}, followed by AgNP1 at 56.09 ± 0.10% and AgNP3 at 46.72 ± 0.18%. Pairwise comparison of DPPH scavenging activity in each concentration of AgNPs and ascorbic acid through

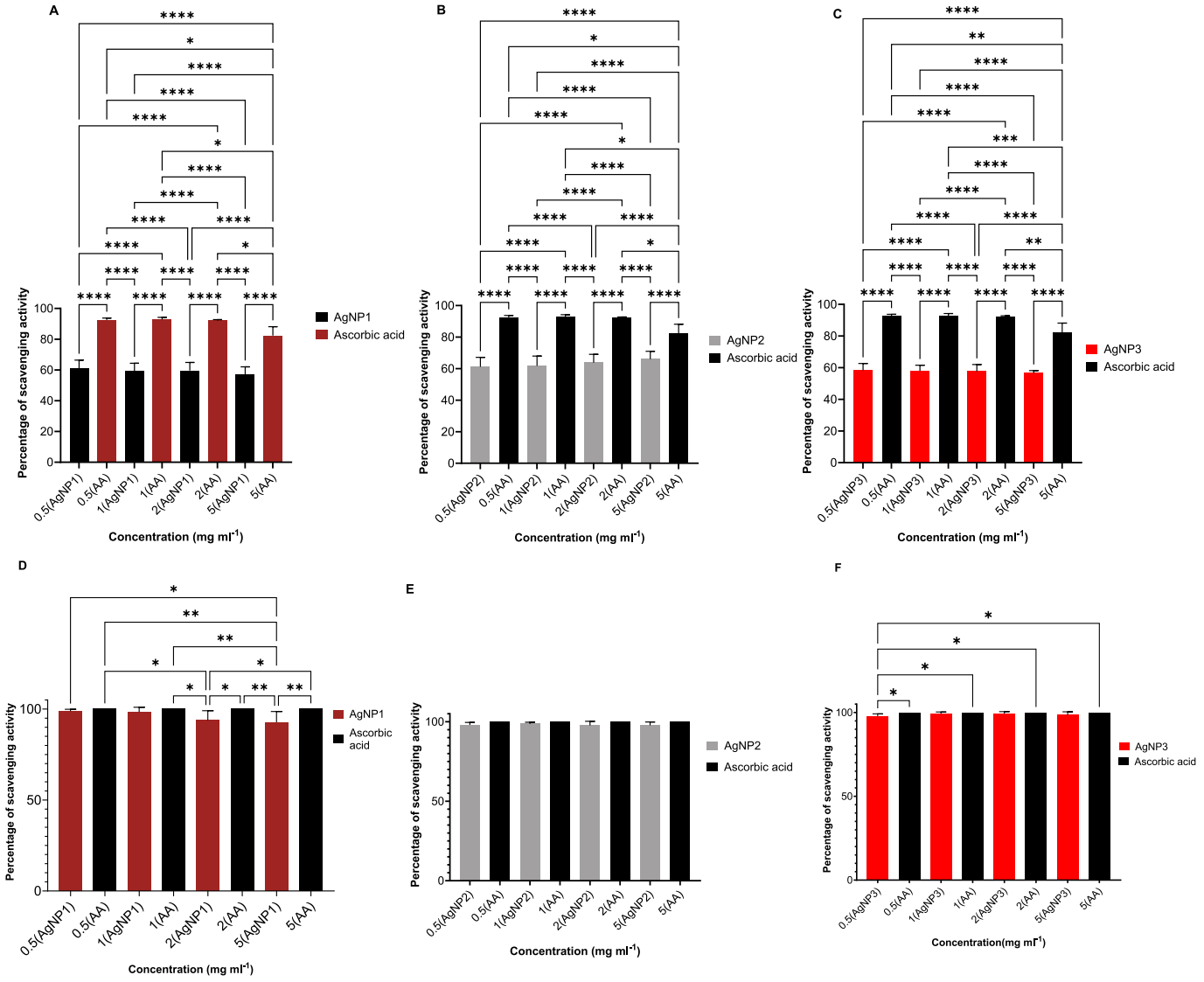

Fig. 3. Antioxidant activity of biosynthesized AgNPs, where **A, B and C** represent DPPH (2,2-diphenyl-1-picrylhydrazyl)-mediated free radical scavenging activity of AgNP1, AgNP2, and AgNP3 at different concentrations (0.5–5 mg mL^{-1}) where standard antioxidant ascorbic acid was taken as control. **D, E, and F** represent Hydrogen peroxide (H_2O_2) mediated hydroxyl (•OH) radical scavenging activity of AgNP1, AgNP2, and AgNP3 at identical concentrations. Results are presented as mean ± standard deviation (n = 3). Statistical significance compared to the control was evaluated by one-way ANOVA.

one-way ANOVA using Šídák's multiple comparisons tests is detailed in Table S1, Table S2, and Table S3, respectively. This is comparable to other studies of AgNP green synthesis. For instance, *Allophylus cobbe*-mediated AgNPs reported by Gurunathan et al. [11] demonstrated scavenging activities in a similar range (~60–70%) but only at higher concentrations (≥10 mg mL^{-1}), highlighting the efficiency of AgNPs synthesized in this study at lower concentrations. Interestingly, the antioxidant performance of AgNP3 synthesized by *Staphylococcus* sp. BSP3 aligns with findings by Sadowski et al. [59], who observed similar scavenging activities for AgNPs synthesized using bacterial cell-free extracts, suggesting that the exopolysaccharides (EPSs) produced by the bacteria in the cell-free extracts may enhance the stability and activity of the NPs. However, ascorbic acid remained the most potent antioxidant in all cases, consistent with prior studies, such as Ahmed et al. [9], where synthetic antioxidants generally outperform natural NP-based systems in scavenging activities.

Overall, the results demonstrate that AgNP2, synthesized by the cell-free extract of thermotolerant *P. alcaligenes* Med1, exhibited the highest DPPH radical scavenging activity among the biosynthesized AgNPs even at very low concentrations, potentially due to its smaller size, optimum heterogeneity, and enhanced stability, as indicated in the TEM and DLS analyses. However, all AgNPs showed lower scavenging activity than ascorbic acid, which acted as the positive control.

3.2.2. Hydrogen peroxide scavenging activity

The OH radical (•OH) scavenging activity of the biosynthesized silver nanoparticles (AgNP1, AgNP2, and AgNP3) was assessed and compared with ascorbic acid as the standard antioxidant. The assay was performed at various concentrations of 0.5, 1, 2, and 5 mg mL^{-1}. Among the tested samples, ascorbic acid demonstrated the highest scavenging activity, consistently reaching 100% across all tested concentrations, serving as the positive control (Fig. 3D–F). For the AgNPs, all samples showed excellent scavenging activities, with values above 92% at all concentrations. Notably, the scavenging activity varied slightly among the AgNPs. At 0.5 mg mL^{-1}, AgNP1 exhibited the highest scavenging activity (98.83 ± 0.04%), followed by AgNP2 (97.99 ± 0.07%) and AgNP3 (97.76 ± 0.02%). At 1 mg mL^{-1}, all AgNPs showed enhanced scav-

enging activity, with AgNP1 achieving the maximum (99.88 ± 0.08%), followed by AgNP3 (99.59 ± 0.04%) and AgNP2 (99.06 ± 0.05 %). Interestingly, at higher concentrations (2 and 5 mg mL^{-1}), the scavenging activity of AgNP2 and AgNP3 remained consistently high, with AgNP3 maintaining superior activity (99.42 ± 0.03% at 2 mg mL^{-1} and 99.35 ± 0.07% at 5 mg mL^{-1}). AgNP1, however, exhibited a slight decrease in activity at these concentrations (93.61 ± 0.12% and 92.48 ± 0.17%, respectively).

Overall, the results suggest that AgNP3, synthesized by the cell-free extracts of thermotolerant *Staphylococcus* sp. BSP3, displayed superior •OH scavenging activity at higher concentrations, closely followed by AgNP2 synthesized by *P. alcaligenes* Med1. The H_2O_2 scavenging activity of AgNP3 synthesized by *Staphylococcus* sp. BSP3 (99.42 ± 0.03% at 2 mg mL^{-1}) was particularly noteworthy, surpassing the activity of AgNPs synthesized by *Streptomyces* sp. as reported by Karthik et al. [34], where scavenging efficiencies peaked at ~85% under similar assay conditions. Similarly, AgNP2 synthesized by *P. alcaligenes* Med1 demonstrated excellent activity at 5 mg mL^{-1} (97.76 ± 0.07%), outperforming AgNPs produced using *B. amyloliquefaciens* in earlier studies [60]. Pairwise comparison of H_2O_2 scavenging activity in each concentration of AgNPs and ascorbic acid through one-way ANOVA is detailed in Table S4, Table S5, and Table S6, respectively. It is also observed from the statistical analysis using one-way ANOVA with Šídák's multiple comparisons that AgNP2 and AgNP3 had H_2O_2 scavenging activities not significantly different from ascorbic acid at most concentrations ($p > 0.05$). Only AgNP1 at 5 mg mL^{-1} exhibited a significant reduction when compared to ascorbic acid (adjusted ρ-value 0.0033). It is consistent with its slightly reduced performance. These results support the comparable antioxidant potential of AgNP2 and AgNP3 to the positive control.

The slight decrease in the activity of AgNP1 at higher concentrations may be attributed to particle aggregation, as supported by previous studies like Ravindran et al. [13], where larger particle sizes and higher polydispersity indices correlated with reduced antioxidant performance. The consistency in scavenging activity for AgNP2 and AgNP3 suggests that their smaller sizes and higher zeta potentials (as observed in DLS and TEM analyses) contribute to enhanced reactivity and stability. Despite the slight differences among the AgNPs, all samples exhibited significant antioxidant potential, comparable to the control ascorbic acid. The enhanced performances of AgNP2 and AgNP3 at higher concentrations could be attributed to the unique reducing and capping agents secreted by the cell-free extracts of the hot spring origin bacteria *P. alcaligenes* Med1 and *Staphylococcus* sp. BSP3, which may impact superior electron-donating capability. This aligns with the recent study by Ansari et al. [61], where bacterial EPS and proteins were found to enhance the activity and stability of biosynthesized AgNPs.

3.2.3. Agar well diffusion assay

The antibacterial activity of the biosynthesized silver nanoparticles (AgNP1, AgNP2, and AgNP3) was evaluated using the agar well diffusion assay. *P. putida* (gram-negative) and *B. cereus* (gram-positive) were used as test organisms. Zones of inhibition (ZOI) were measured to assess the antibacterial efficacy of the unpurified nanoparticles at various concentrations (100 µL, 200 µL, and 300 µL per well), with cefotaxime and $AgNO_3$ serving as positive and negative controls, respectively. In common bacterial infections like urinary tract infections, pneumonia, sepsis or central nervous system (CNS) infections, Cefotaxime is used widely in clinical practice. Furthermore, in previous reports for evaluation of antibacterial performance of novel nanoformulations, Cefotaxime is frequently used as positive controls [62] due to its well-known inhibition of bacterial cell wall synthesis by binding to penicillin-binding proteins (PBPs) [63,64]. The results demonstrated that all AgNP samples exhibited significant antibacterial activity, with a clear ZOI observed around the wells. The efficacy of the AgNPs varied depending on the bacterial strain, nanoparticle type, and concentration. For *P. putida*, AgNP3 was synthesized using *Staphylococcus* sp. BSP3 exhibited the largest zone of inhibition (ZOI) across all tested concentrations, indicating the highest antibacterial potential. At 300 µL, AgNP3 produced a ZOI of approximately 18 ± 0.5 mm, followed by AgNP2 with 16 ± 0.4 mm and AgNP1 with 14 ± 0.3 mm. For *B. cereus*, a similar trend was observed, with AgNP3 showing the highest activity (19 ± 0.6 mm at 300 µL), followed by AgNP2 (17 ± 0.4 mm) and AgNP1 (15 ± 0.4 mm).

The enhanced antibacterial activity of AgNP3 can be attributed to its smaller particle size (8.4 ± 5.2 nm), higher colloidal stability (as indicated by its zeta potential of −25.7 mV), and less heterogeneity. The increased surface area of smaller nanoparticles likely enhances their interaction with bacterial cell walls, leading to more effective antibacterial activity. These findings align with previous studies, such as those by Babayevska et al. [65] on facile AgNP synthesis and Mohammed et al. [66] on green synthesized AgNPs from *Acinetobacter calcoaceticus*, which reported that smaller, well-dispersed AgNPs exhibit superior antibacterial efficacy. Cefotaxime, a third-generation cephalosporin wide-range antibiotic [67] used as a positive control, produced the largest ZOIs against both bacteria, averaging 20 ± 0.2 mm. $AgNO_3$ used as a negative control exhibited negligible antibacterial activity, confirming that the observed effects were due to the biosynthesized AgNPs. The initial results from the agar well diffusion assay highlight the effectiveness of biosynthesized AgNPs as antibacterial agents, particularly AgNP3 synthesized using *Staphylococcus* sp. BSP3. The observed differences in antibacterial activity among the AgNPs suggest that bacterial strain characteristics play a crucial role in determining the physicochemical properties of the nanoparticles because of the different bioactive enzymes or EPS that they produce, which affect their biological activities [68]. These findings emphasize the potential of biosynthesized AgNPs in addressing antimicrobial resistance, as previously discussed by Parmar et al. [69].

3.2.4. Bacterial cell viability assay

The antibacterial activity of the biosynthesized silver nanoparticles (AgNP1, AgNP2, and AgNP3) and the standard antibiotic cefotaxime was evaluated against *B. cereus* and *P. putida* through cell viability assays. The results demonstrated a concentration-dependent reduction in bacterial cell viability for all tested agents, with significant variations in efficacy between the nanoparticles and the control. Among the silver nanoparticles, AgNP2 exhibited the highest antibacterial activity against both bacterial strains, particularly at 1 mg mL^{-1}, where *P. putida* showed near-complete cell death (0.74%), and *B. cereus* exhibited 26.32% viability. At 10 mg mL^{-1}, the cell viability for both strains was reduced to 3.40% (*B. cereus*) and 1.08% (*P. putida*), showcasing its potent bactericidal effects. AgNP3 demonstrated moderate antibacterial activity, with *P. putida* showing higher sensitivity than *B. cereus,* particularly at lower concentrations. At 10 mg mL^{-1}, *P. putida* exhibited 11.66% viability, while *B. cereus* showed 5.98%. AgNP1 was the least effective among the nanoparticles, with *B. cereus* showing 1.53% viability and *P. putida* 32.83% viability at 10 mg mL^{-1}, indicating reduced efficacy against the Gram-negative strain. In comparison, the control cefotaxime exhibited moderate antibacterial activity but was less effective than the biosynthesized nanoparticles. At 0.5 mg mL^{-1}, *B. cereus* and *P. putida* showed viabilities of 27.94% and 49.22%, respectively. Even at higher concentrations (10 mg mL^{-1}), *B. cereus* exhibited 35.61% viability (Fig. 4), reflecting its resistance to cefotaxime compared to the nanoparticles. *P. putida* showed 19.35% viability at the same concentration, indicating moderate sensitivity (Fig. 5).

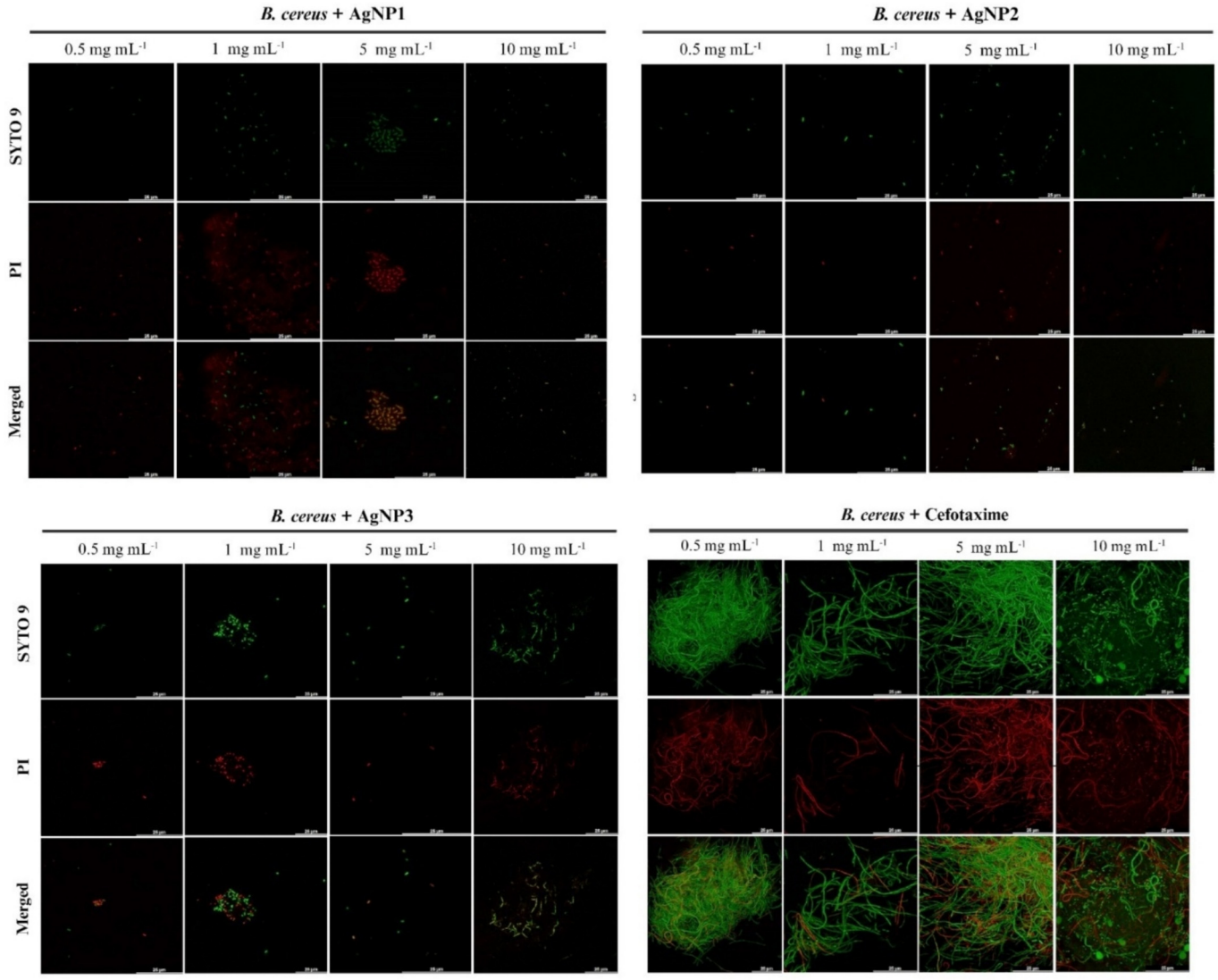

Fig. 4. LIVE/DEAD BacLight cell viability assay confocal microscopy images showing the action of the AgNP1, AgNP2, and AgNP3 on gram-positive *B. cereus* compared to standard antibiotic Cefotaxime. The merged images of SYTO 9/PI emit green fluorescence for viable cells and red fluorescence for damaged/ dead cells. (For interpretation of the references to color in this figure legend, the reader is referred to the web version of this article.)

The observed antibacterial efficacy of the biosynthesized AgNPs in the cell viability assay correlates with their physicochemical properties, as revealed in the TEM, DLS, and FTIR analyses. Among the tested nanoparticles, AgNP2 exhibited the highest antibacterial activity, which may be attributed to its optimal size (10.78 ± 6.40 nm), moderate heterogeneity, and relatively high zeta potential (−22.3 mV), indicating enhanced colloidal stability. These properties likely facilitated effective interactions with bacterial cell walls, disrupting their integrity and promoting ROS generation. Similarly, AgNP3 demonstrated considerable activity, particularly against gram-negative *P. putida,* which may be linked to its smaller size (8.40 ± 5.21 nm) and the presence of stabilizing biomolecules such as hydroxyl and amide groups, as confirmed by FTIR. This smaller size may enhance its penetration into bacterial membranes, contributing to its bactericidal effects. On the other hand, AgNP1, with the largest size (20.82 ± 12.56 nm) and higher polydispersity, showed lower antibacterial activity, especially against *P. putida.* The increased size and heterogeneity of AgNP1 might hinder its ability to interact with bacterial cells, reducing its efficacy effectively. Additionally, the FTIR data revealed the role of polysaccharides and proteins in nanoparticle stabilization, which may have influenced their biological activity. The superior performance of AgNP2 and AgNP3 compared to AgNP1 emphasizes the critical influence of nanoparticle size, shape, and surface properties on their antibacterial potential, highlighting the importance of controlled synthesis to optimize their efficacy against pathogenic bacteria. These findings suggest that smaller, monodispersed nanoparticles with strong electrostatic stabilization, such as AgNP2 and AgNP3, are better suited for antibacterial applications. Recently, Yalcinoz et al. [70] reported biosynthesis of AgNPs produced by a thermotolerant strain *Anoxybacillus sp.* D401a, where TEM analysis revealed the nanoparticle size of 24–57 nm of spherical AgNPs produced. Recently, Srimathi et al. [71] demonstrated the biogenic synthesis of AgNPs with culture supernatant of multidrug-resistant bacterial strains like *P. aeruginosa* ATCC 27853, *Acinetobacter baumannii* ATCC17978, and *Escherichia coli* ATCC 25922. All these strains are reported to produce spherical AgNPs within the range of 159.9 ± 12.8 nm to 168.4 ± 10.3 nm size. Cell-free supernatant of *Haematococcus pluvialis* is also reported to produce quasi-spherical AgNPs within the range of 30–50 nm [72]. In the present study, TEM analysis displayed a narrow size distribution of AgNPs which are substantially more homogeneously

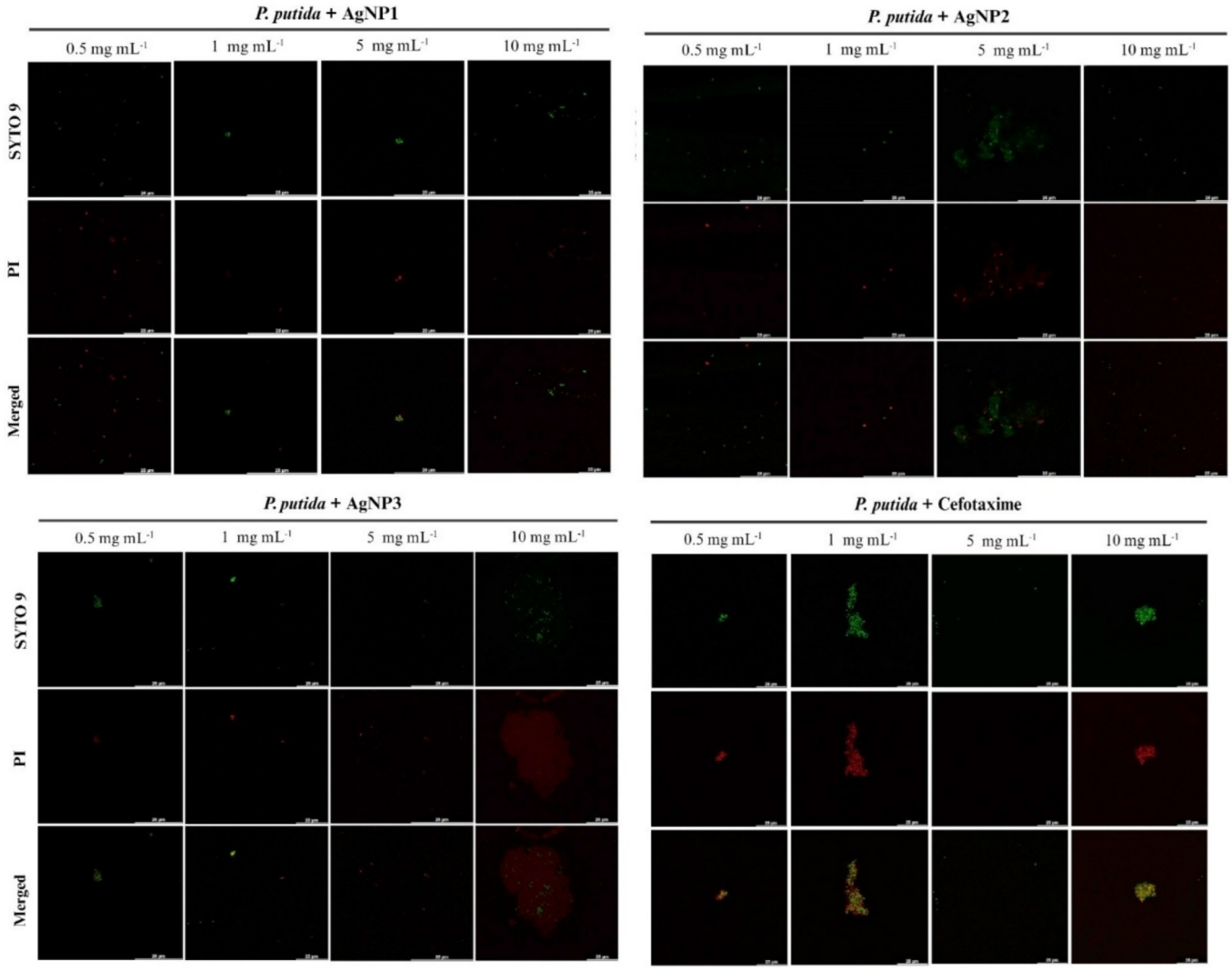

Fig. 5. LIVE/DEAD BacLight cell viability assay confocal microscopy images showing the action of the AgNP1, AgNP2, and AgNP3 on gram-negative *P. putida* compared to the positive control Cefotaxime. The merged images of SYTO 9/PI emit green fluorescence for viable cells and red fluorescence for damaged/ dead cells. (For interpretation of the references to colo in this figure legend, the reader is referred to the web version of this article.)

uniform than those previously reported studies. Uniformity in nanoparticle size enhances colloidal stability by minimizing aggregation potential. That also ensures consistent physicochemical and biological behavior of nanoparticles. Previous works have already demonstrated that homogeneous nanoparticle size leads to improved cellular uptake, reproducible optical properties, and reliable pharmacokinetics in biomedical systems [73,74,75].

Overall, the biosynthesized AgNPs, particularly AgNP2 and AgNP3, outperformed cefotaxime in reducing bacterial cell viability, showcasing their potential as effective alternatives to traditional antibiotics (Fig. 6). The superior activity of AgNP2 highlights its promising application in combating bacterial infections, including those caused by Gram negative strains, which are generally more resistant to conventional antibiotics. AgNP2 demonstrating superior antibacterial activity may be attributed to its optimal size and surface properties. This observation aligns with findings by Loo et al. [76], who reported that green-synthesized AgNPs with an average size of approximately 4.06 nm exhibited significant antibacterial activity against gram-negative foodborne pathogens, suggesting that smaller nanoparticles possess enhanced antimicrobial properties. Furthermore, specific functional groups on the nanoparticle surface play a crucial role in their stability and interaction with bacterial cells. Our FTIR analysis revealed hydroxyl and amide groups contributing to nanoparticle stabilization, consistent with the work of Ahmed et al. [9], who identified similar functional groups in biogenic AgNPs synthesized using plant extracts, correlating these groups with enhanced antibacterial efficacy. Additionally, the zeta potential of the AgNPs significantly impacted their antibacterial potential. AgNP2 and AgNP3, with higher negative zeta potentials, exhibited better colloidal stability and stronger interactions with bacterial membranes, as supported by the findings of Bogdanova et al. [77], who emphasized the importance of surface charge in nanoparticle stability and antibacterial activity. AgNP1 showed relatively lower antibacterial activity, likely due to its larger size and higher heterogeneity, which might hinder its ability to effectively disrupt bacterial membranes. Similar observations were reported by Menichetti et al. [78], where AgNPs with larger diameters displayed reduced bactericidal activity compared to their smaller counterparts. The differences in efficacy between gram-positive *B. cereus* and gram-negative *P. putid*a observed in our study are also consistent with prior studies, which attribute the higher resistance of gram-positive bacteria to their thick peptidoglycan layer, reducing nanoparticle penetration. Furthermore, *P. putida* displayed

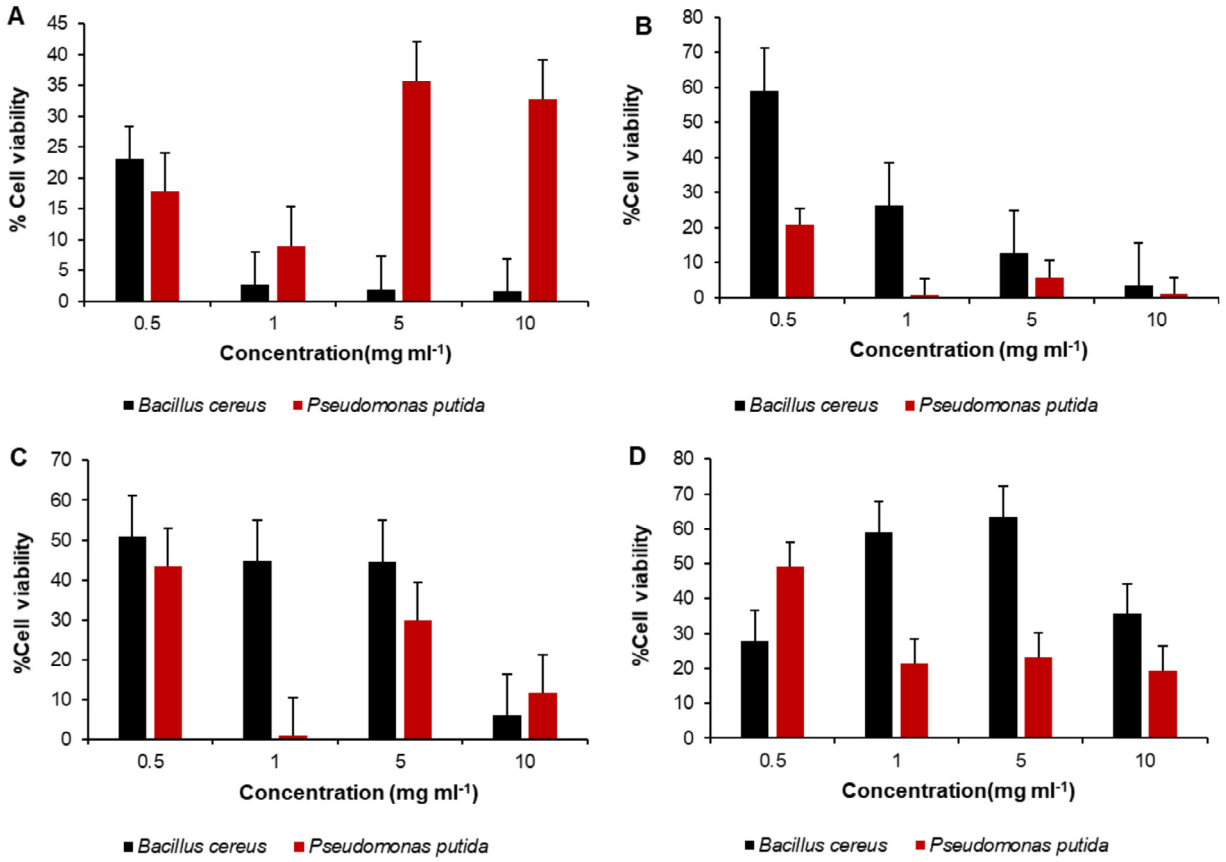

Fig. 6. Viability percentages of *B. cereus* and *P. putida* following treatment with biosynthesized AgNPs and control antibiotic. (A–C) Histogram showing the percentage of viable bacterial cells after exposure to AgNP1, AgNP2, and AgNP3, respectively, as measured by LIVE/DEAD™ BacLight™ fluorescence assay. (D) Positive control using 20 µL of cefotaxime treatment. Data represent means ± SD from three independent experiments. Live and dead cell populations were quantified via confocal microscopy and ImageJ analysis.

higher sensitivity to the nanoparticles than the control cefotaxime, highlighting the potential of biosynthesized AgNPs in addressing Gram negative bacterial infections, which are often more resistant to conventional antibiotics [79]. The enhanced efficacy of AgNP2 and AgNP3, particularly against *P. putida*, underscores the significance of controlled synthesis methods to optimize nanoparticle size, surface properties, and stability. These properties collectively influence the ability of AgNPs to generate ROS and disrupt bacterial membranes, as reported by Reidy et al. [22].

However, one limitation of the present study is the lack of cytotoxicity assessment on mammalian cell lines, which is essential for evaluating the safety and translational applicability of the synthesized nanoparticles. Future studies should incorporate comprehensive *in vitro* and *in vivo* toxicity evaluations to validate the biomedical potential of these AgNPs. In conclusion, the findings from this study reinforce the potential of biosynthesized AgNPs as effective antimicrobial agents, particularly against drug-resistant bacterial strains.

4. Conclusions

In this study, AgNPs were biosynthesized using cell-free extracts from thermotolerant bacterial strains *B. haynesii* CamB6, *Pseudomonas alcaligenes* Med1, and *Staphylococcus* sp. BSP3. The nanoparticles were characterized using UV–Vis, FTIR, TEM, DLS, and zeta potential analyses, revealing that AgNP2 possessed the smallest size, highest colloidal stability, and most uniform spherical morphology. FTIR spectra confirmed the presence of functional groups such as hydroxyl and amide, supporting the involvement of bacterial biomolecules like proteins, phenolics, and polysaccharides in nanoparticle reduction and stabilization. Biological evaluations demonstrated that all three AgNPs exhibited antioxidant activity, with AgNP2 and AgNP3 showing stronger free radical scavenging capacity. In antibacterial assays, AgNP2 and AgNP3 significantly reduced bacterial viability and outperformed cefotaxime against both *P. putida* and *B. cereus*. AgNP2 showed the highest antibacterial activity, likely due to its smaller particle size, uniform shape, and higher surface charge, which collectively enhance interaction with bacterial membranes and promote ROS-mediated damage. This study demonstrates that thermotolerant bacterial strains provide a robust and eco-friendly platform for synthesizing biologically active AgNPs with promising antioxidant and antibacterial properties. While these findings highlight their biomedical potential, the lack of cytotoxicity assessment on mammalian cells remains a limitation. Future work will focus on evaluating biocompatibility and exploring therapeutic applications.

CRediT authorship contribution statement

Aparna Banerjee: Writing – review & editing, Writing – original draft, Supervision, Resources, Project administration, Methodology, Funding acquisition, Formal analysis, Conceptualization. **Ismael Herrera-Vargas:** Writing – original draft, Software, Investigation, Formal analysis, Data curation. **Mario E. Flores:** Writing – review & editing, Resources, Investigation, Formal analysis, Data curation. **Francisca Valenzuela:** Writing – review & editing, Investigation, Data curation. **Srijan Banerjee:** Writing – review & editing, Visualization, Formal analysis, Data curation.

Financial support

AB, IH-V, FV, and SB acknowledge Fondecyt Regular 1231917 by ANID, Govt. of Chile for the funding.

Declaration of competing interest

The authors declare that they have no known competing financial interests or personal relationships that could have appeared to influence the work reported in this paper.

Acknowledgements

The authors are thankful to FONDEQUIP-ANID EQM200122 for the confocal microscopy.

Supplementary material

https://doi.org/10.1016/j.ejbt.2025.100698.

Data availability

Data will be made available on request.

References

[1] Malik S, Muhammad K, Waheed Y. Emerging applications of nanotechnology in healthcare and medicine. Molecules 2023;28(18):6624. https://doi.org/10.3390/molecules28186624. PMid: 37764400.

[2] Mandvi Singh PP, Ballal S, et al. Construction of a 3D flower-like NiO/Mn_3O_4 heterojunction using Tulsi leaf extract for enhanced photodegradation of thiamethoxam pesticide and organic dyes under direct sunlight. Mater Adv 2024;5(20):8097–110. https://doi.org/10.1039/D4MA00708E.

[3] Sodhi RS, Singh PP, Lal B, et al. Biogenic synthesis of ZnO nanoparticles using *Polystichum squarrosum* extract and its applications as anti-oxidant, anti-diabetic agent and industrial wastewater treatment. Emerg Mater 2024;7:285–98. https://doi.org/10.1007/s42247-023-00589-7.

[4] Kumari V, Kaushal S, Singh PP. Green synthesis of a CuO/rGO nanocomposite using a *Terminalia arjuna* bark extract and its catalytic activity for the purification of water. Mater Adv 2022;3(4):2170–84. https://doi.org/10.1039/D1MA00993A.

[5] Mahajan M, Kumar S, Gaur J, et al. Role of cellulose, phenolic compounds, and water-soluble proteins in ZnO nanoparticle synthesis using *Mangifera indica* leaf extract for photocatalytic and antioxidant investigations. Colloids Surf A Physicochem Eng Asp 2025;720:137066. https://doi.org/10.1016/j.colsurfa.2025.137066.

[6] Mahajan M, Kumar R, Gaur J, et al. Green synthesis of ZnO nanoparticles using *Justicia adhatoda* for photocatalytic degradation of malachite green and reduction of 4-nitrophenol. RSC Adv 2025;15(4):2958–80. https://doi.org/10.1039/D4RA08632E.

[7] Kumar V, Singh Y, Kaushal S, et al. Bioinspired synthesis of copper oxide nanoparticles using aqueous extracts of *Cladophora glomerata* (L.) Kuetz and their potential biomedical applications. Bioprocess Biosyst Eng 2025;48:633–46. https://doi.org/10.1007/s00449-025-03133-5. PMid: 39928099.

[8] Singh H, Du J, Singh P, et al. Ecofriendly synthesis of silver and gold nanoparticles by *Euphrasia officinalis* leaf extract and its biomedical applications. Artif Cells Nanomed Biotechnol 2018;46(6):1163–70. https://doi.org/10.1080/21691401.2017.1362417. PMid: 28784039.

[9] Ahmed S, Annu, Ikram S, et al. Biosynthesis of gold nanoparticles: A green approach. J Photochem Photobiol B Biol 2016;161:141–53. https://doi.org/10.1016/j.jphotobiol.2016.04.034. PMid: 27236049.

[10] Murugan S, Senthilvelan T, Govindasamy M, et al. A comprehensive review on exploring the potential of phytochemicals and biogenic nanoparticles for the treatment of antimicrobial-resistant pathogenic bacteria. Curr Microbiol 2025;82(2):90. https://doi.org/10.1007/s00284-025-04064-w. PMid:39825917.

[11] Gurunathan S, Han JW, Kwon D-N, et al. Enhanced antibacterial and anti-biofilm activities of silver nanoparticles against Gram-negative and Gram-positive bacteria. Nanoscale Res Lett 2014;9(1):373. https://doi.org/10.1186/1556-276X-9-373. PMid: 25136281.

[12] Banerjee A, Das D, Andler R, et al. Green synthesis of silver nanoparticles using exopolysaccharides produced by *Bacillus anthracis* PFAB2 and its biocidal property. J Polym Environ 2021;29(8):2701–9. https://doi.org/10.1007/s10924-021-02051-3.

[13] Ravindran A, Chandran P, Khan SS. Biofunctionalized silver nanoparticles: Advances and prospects. Colloids Surf B Biointerfaces 2013;105:342–52. https://doi.org/10.1016/j.colsurfb.2012.07.036. PMid:2 3411404.

[14] Dheyab MA, Aziz AA, Jameel MS, et al. Sustainable green synthesis of silver nanoparticles for safer biomedical application. J Environ Chem Eng 2025;13(2):115998. https://doi.org/10.1016/j.jece.2025.115998.

[15] Taran M, Rad M, Alavi M. Antibacterial activity of copper oxide (CuO) nanoparticles biosynthesized by *Bacillus* sp. FU4: Optimization of experiment design. Pharm Sci 2014;23(3):198–206. https://doi.org/10.15171/PS.2017.30.

[16] Das CGA, Sharma R, Singh A, et al. Antibacterial activity of silver nanoparticles (biosynthesis): A short review on recent advances. Biocatal Agric Biotechnol 2020;27:101593. https://doi.org/10.1016/j.bcab.2020.101593.

[17] Galdiero S, Falanga A, Vitiello M, et al. Silver nanoparticles as potential antiviral agents. Molecules 2011;16(10):8894–918. https://doi.org/10.3390/molecules16108894. PMid: 22024958.

[18] Pangli H, Vatanpour S, Hortamani S, et al. Incorporation of silver nanoparticles in hydrogel matrices for controlling wound infection. J Burn Care Res 2021;42(4):785–93. https://doi.org/10.1093/jbcr/iraa205. PMid: 33313805.

[19] Gondil VS, Kalaiyarasan T, Bharti VK, et al. Antibiofilm potential of Seabuckthorn silver nanoparticles (SBT@AgNPs) against *Pseudomonas aeruginosa*. 3 Biotech 2019;9(11):402. https://doi.org/10.1007/s13205-019-1947-6. PMid: 31681523.

[20] Khairnar SV, Das A, Oupický D, et al. Strategies to overcome antibiotic resistance: Silver nanoparticles and vancomycin in pathogen eradication. RSC Pharm 2025;2(3):455–79. https://doi.org/10.1039/D4PM00314D.

[21] Singh Y, Kaushal S, Sodhi RS. Biogenic synthesis of silver nanoparticles using cyanobacterium *Leptolyngbya* sp. WUC 59 cell-free extract and their effects on bacterial growth and seed germination. Nanoscale Adv 2020;2(9):3972–82. https://doi.org/10.1039/D0NA00357C. PMid: 36132754.

[22] Reidy B, Haase A, Luch A, et al. Mechanisms of silver nanoparticle release, transformation and toxicity: A critical review of current knowledge and recommendations for future studies and applications. Materials 2013;6(6):2295–350. https://doi.org/10.3390/ma6062295. PMid: 28809275.

[23] Casals E, Gusta MF, Bastus N, et al. Silver nanoparticles and antibiotics: A promising synergistic approach to multidrug-resistant infections. Microorganisms 2025;13(4):952. https://doi.org/10.3390/microorganisms13040952. PMid: 40284788.

[24] Yamanaka M, Hara K, Kudo J. Bactericidal actions of a silver ion solution on *Escherichia coli*, studied by energy-filtering transmission electron microscopy and proteomic analysis. Appl Environ Microbiol 2005;71(11):7589–93. https://doi.org/10.1128/AEM.71.11.7589-7593.2005. PMid: 16269810.

[25] Banerjee A, Roy RK, Sarkar S, et al. Synthesis of hot spring origin bacterial cell wall polysaccharide-based copper nanoparticles with antibacterial property. Electron J Biotechnol 2024;68:11–9. https://doi.org/10.1016/j.ejbt.2023.11.005.

[26] Banerjee A, Das D, Rudra SG, et al. Characterization of exopolysaccharide produced by *Pseudomonas* sp. PFAB4 for synthesis of EPS-coated AgNPs with antimicrobial properties. J Polym Environ 2020;28(1):242–56. https://doi.org/10.1007/s10924-019-01602-z.

[27] Banerjee A, Mohammed Breig SJ, Gómez A, et al. Optimization and characterization of a novel exopolysaccharide from *Bacillus haynesii* CamB6 for food applications. Biomolecules 2022;12(6):834. https://doi.org/10.3390/biom12060834. PMid: 35740959.

[28] Sarkar S, Cabrera-Barjas G, Singh RN, et al. Unveiling a novel exopolysaccharide produced by *Pseudomonas alcaligenes* Med1 isolated from a Chilean hot spring as biotechnological additive. Sci Rep 2024;14(1):25058. https://doi.org/10.1038/s41598-024-74830-6. PMid: 39443539.

[29] Banerjee S, Cabrera-Barjas G, Tapia J, et al. Characterization of Chilean hot spring-origin *Staphylococcus* sp. BSP3 produced exopolysaccharide as biological additive. Nat Prod Bioprospect 2024;14(1):15. https://doi.org/10.1007/s13659-024-00436-0. PMid: 38310179.

[30] Ghodake G, Kim M, Sung J, et al. Extracellular synthesis and characterization of silver nanoparticles—Antibacterial activity against multidrug-resistant bacterial strains. Nanomaterials 2020;10(2):360. https://doi.org/10.3390/nano10020360. PMid: 32092941.

[31] Singh P, Mijakovic I. Strong antimicrobial activity of silver nanoparticles obtained by the green synthesis in *Viridibacillus* sp. extracts. Front Microbiol 2022;13:820048. https://doi.org/10.3389/fmicb.2022.820048. PMid: 35250934.

[32] Nas F, Aissaoui N, Mahjoubi M, et al. A comparative GC–MS analysis of bioactive secondary metabolites produced by halotolerant *Bacillus* spp. isolated from the Great Sebkha of Oran. Int Microbiol 2021;24(3):455–70. https://doi.org/10.1007/s10123-021-00185-x. PMid: 34100180.

[33] Jacob JA, Mahal HS, Biswas N, et al. Role of phenol derivatives in the formation of silver nanoparticles. Langmuir 2008;24(2):528–33. https://doi.org/10.1021/la702073r. PMid: 18095719.

[34] Ansari MA, Asiri SMM, Alzohairy MA, et al. Biofabricated fatty acids-capped silver nanoparticles as potential antibacterial, antifungal, antibiofilm and anticancer agents. Pharmaceuticals 2021;14(2):139. https://doi.org/10.3390/ph14020139. PMid: 33572296.

[35] Ashrafi-Saiedlou S, Rasouli-Sadaghiani M, Fattahi M, et al. Biosynthesis and characterization of iron oxide nanoparticles fabricated using cell-free supernatant of *Pseudomonas fluorescens* for antibacterial, antifungal, antioxidant, and photocatalytic applications. Sci Rep 2025;15(1):1018. https://doi.org/10.1038/s41598-024-84974-0. PMid: 39762412.

[36] Fedorova MS, Mironova AV, Kayumov AR, et al. Cell-free supernatant of *Staphylococcus aureus* culture increases antimicrobials susceptibility of *Pseudomonas aeruginosa*. Opera Medica et Physiologica 2022;9(3):113–20. https://doi.org/10.24412/2500-2295-2022-3-113-120.
[37] Siriwardana K, Wang A, Gadogbe M, et al. Studying the effects of cysteine residues on protein interactions with silver nanoparticles. J Phys Chem C 2015;119(5):2910–6. https://doi.org/10.1021/jp512440z. PMid: 26207157.
[38] Atalah J, Espina G, Blamey L, et al. Advantages of using extremophilic bacteria for the biosynthesis of metallic nanoparticles and its potential for rare earth element recovery. Front Microbiol 2022;13:855077. https://doi.org/10.3389/fmicb.2022.855077. PMid: 35387087.
[39] Focardi S, Pepi M, Landi G, et al. Hexavalent chromium reduction by whole cells and cell-free extract of the moderate halophilic bacterial strain *Halomonas* sp. TA-04. Int Biodeter Biodegr 2012;66(1):63–70. https://doi.org/10.1016/j.ibiod.2011.11.003.
[40] Shimada K, Fujikawa K, Yahara K, et al. Antioxidative properties of xanthan on the autoxidation of soybean oil in cyclodextrin emulsion. J Agric Food Chem 1992;40(6):945–8. https://doi.org/10.1021/jf00018a005.
[41] Ruch RJ, Cheng S, Klaunig JE. Prevention of cytotoxicity and inhibition of intercellular communication by antioxidant catechins isolated from Chinese green tea. Carcinogenesis 1986;10(6):1003–8. https://doi.org/10.1093/carcin/10.6.1003. PMid: 2470525.
[42] Chavez-Esquivel G, Cervantes-Cuevas H, Ybieta-Olvera LF, et al. Antimicrobial activity of graphite oxide doped with silver against *Bacillus subtilis*, *Candida albicans*, *Escherichia coli*, and *Staphylococcus aureus* by agar well diffusion test: Synthesis and characterization. Mater Sci Eng C 2021;123:111934. https://doi.org/10.1016/j.msec.2021.111934. PMid: 33812573.
[43] Gallagher SR. Digital image processing and analysis with ImageJ. Curr Protoc Essent Lab Tech 2014;9(1):A.3C.1–A.3C.29. https://doi.org/10.1002/9780470089941.eta03cs9.
[44] Saha N, Trivedi P, Dutta Gupta S. Surface plasmon resonance (SPR) based optimization of biosynthesis of silver nanoparticles from rhizome extract of *Curculigo orchioides* Gaertn. and its antioxidant potential. J Clust Sci 2016;27(6):1893–912. https://doi.org/10.1007/s10876-016-1050-7.
[45] Kaimuangpak K, Tamprasit K, Date A, et al. Synthesis of bioactive spherical silver nanoparticles with surface plasmon resonance using ethanolic twig extract of *Cratoxylum formosum* ssp. *pruniflorum*. J Drug Deliv Sci Technol 2023;88:104897. https://doi.org/10.1016/j.jddst.2023.104897.
[46] Gusrizal G, Santosa SJ, Kunarti ES, et al. Synthesis of silver nanoparticles by reduction of silver ion with m-hydroxybenzoic acid. Asian J Chem 2017;29(7):1417–22. https://doi.org/10.14233/ajchem.2017.20436.
[47] Marguier A, Lakard S, Soraru C, et al. Modulation by surroundings of the antibacterial efficiency of silver in water environments. J Nanopart Res 2019;21(6):129. https://doi.org/10.1007/s11051-019-4544-z.
[48] Choi Y, Kim H-A, Kim K-W, et al. Comparative toxicity of silver nanoparticles and silver ions to *Escherichia coli*. J Environ Sci 2018;66:50–60. https://doi.org/10.1016/j.jes.2017.04.028. PMid: 29628108.
[49] Chen Y, Chen Y, Liu L, et al. Microbial synthesis of 4-hydroxybenzoic acid from renewable feedstocks. Food Chem Mol Sci 2021;3:100059. https://doi.org/10.1016/j.fochms.2021.100059. PMid: 35415641.
[50] Wang K, Pan X, Yang T, et al. Efficient production of salicylic acid through CmeR-P_{cmeO} biosensor-assisted multiplexing pathway optimization in *Escherichia coli*. Biotechnol Biofuels Bioproducts 2025;18(1):40. https://doi.org/10.1186/s13068-025-02637-2. PMid: 40156043.
[51] Karthik L, Kumar G, Kirthi AV, et al. *Streptomyces* sp. LK3 mediated synthesis of silver nanoparticles and its biomedical application. Bioprocess Biosyst Eng 2014;37(2):261–7. https://doi.org/10.1007/s00449-013-0994-3. PMid: 23771163.
[52] Sidhu AK, Verma N, Kaushal P. Role of biogenic capping agents in the synthesis of metallic nanoparticles and evaluation of their therapeutic potential. Front Nanotechnol 2022;3:801620. https://doi.org/10.3389/fnano.2021.801620.
[53] Saeed S, Iqbal A, Ashraf MA. Bacterial-mediated synthesis of silver nanoparticles and their significant effect against pathogens. Environ Sci Pollut Res 2020;27(30):37347–56. https://doi.org/10.1007/s11356-020-07610-0. PMid: 32130634.
[54] Jia Z, Li J, Gao L, et al. Dynamic light scattering: A powerful tool for in situ nanoparticle sizing. Colloids Interfaces 2023;7(1):15. https://doi.org/10.3390/colloids7010015.
[55] Rodriguez-Loya J, Lerma M, Gardea-Torresdey JL. Dynamic light scattering and its application to control nanoparticle aggregation in colloidal systems: A review. Micromachines 2023;15(1):24. https://doi.org/10.3390/mi15010024. PMid: 38258143.
[56] Filippov SK, Khusnutdinov R, Murmiluk A, et al. Dynamic light scattering and transmission electron microscopy in drug delivery: A roadmap for correct characterization of nanoparticles and interpretation of results. Mater Horiz 2023;10(12):5354–70. https://doi.org/10.1039/D3MH00717K.
[57] Danaei M, Dehghankhold M, Ataei S, et al. Impact of particle size and polydispersity index on the clinical applications of lipidic nanocarrier systems. Pharmaceutics 2018;10(2):57. https://doi.org/10.3390/pharmaceutics10020057. PMid: 29783687.
[58] Wang Z, Xiao K, Wang X. Role of coexistence of negative and positive membrane surface charges in electrostatic effect for salt rejection by nanofiltration. Desalination 2018;444:75–83. https://doi.org/10.1016/j.desal.2018.07.010.
[59] Sadowski Z, Maliszewska IH, Grochowalska B, et al. Synthesis of silver nanoparticles using microorganisms. Mater Sci-Pol 2008;26(2):419–24.
[60] Fouad H, Honjie L, Yanmei D, et al. Synthesis and characterization of silver nanoparticles using *Bacillus amyloliquefaciens* and *Bacillus subtilis* to control filarial vector *Culex pipiens pallens* and its antimicrobial activity. Artif Cells Nanomed Biotechnol 2017;45(7):1369–78. https://doi.org/10.1080/21691401.2016.1241793. PMid: 27855517.
[61] Ansari A, Pervez S, Javed U, et al. Characterization and interplay of bacteriocin and exopolysaccharide-mediated silver nanoparticles as an antibacterial agent. Int J Biol Macromol 2018;115:643–50. https://doi.org/10.1016/j.ijbiomac.2018.04.104. PMid: 29689285.
[62] Halawani EM, Hassan AM, Gad El-Rab SM. Nanoformulation of biogenic cefotaxime-conjugated-silver nanoparticles for enhanced antibacterial efficacy against multidrug-resistant bacteria and anticancer studies. Int J Nanomed 2020;15:1889–901. https://doi.org/10.2147/IJN.S236182. PMid: 32256066.
[63] Javaid S, Ahmad NM, Mahmood A, et al. Cefotaxime loaded polycaprolactone based polymeric nanoparticles with antifouling properties for in-vitro drug release applications. Polymers 2021;13(13):2180. https://doi.org/10.3390/polym13132180. PMid: 34209144.
[64] Fontana R, Ligozzi M, Comaglia G. Affinities of cephalosporins for penicillin-binding proteins and their antibacterial activities in the presence of human serum albumin. Clin Microbiol Infect 2000;6(3):82–3. https://doi.org/10.1111/j.1469-0691.2000.tb02052.x.
[65] Babayevska N, Przysiecka Ł, Iatsunskyi I, et al. ZnO size and shape effect on antibacterial activity and cytotoxicity profile. Sci Rep 2022;12(1):8148. https://doi.org/10.1038/s41598-022-12134-3. PMid: 35581357.
[66] Mohammed AM, Hassan KT, Hassan OM. Assessment of antimicrobial activity of chitosan/silver nanoparticles hydrogel and cryogel microspheres. Int J Biol Macromol 2023;233:123580. https://doi.org/10.1016/j.ijbiomac.2023.123580. PMid: 36764343.
[67] Wangoye K, Mwesigye J, Tungotyo M, et al. Chronic wound isolates and their minimum inhibitory concentrations against third generation cephalosporins at a tertiary hospital in Uganda. Sci Rep 2022;12(1):1195. https://doi.org/10.1038/s41598-021-04722-6. PMid: 35075152.
[68] Singh R, Shedbalkar UU, Wadhwani SA, et al. Bacteriagenic silver nanoparticles: Synthesis, mechanism, and applications. Appl Microbiol Biotechnol 2015;99(11):4579–93. https://doi.org/10.1007/s00253-015-6622-1. PMid: 25952110.
[69] Parmar S, Kaur H, Singh J, et al. Recent advances in green synthesis of Ag NPs for extenuating antimicrobial resistance. Nanomaterials 2022;12(7):1115. https://doi.org/10.3390/nano12071115. PMid: 35407234.
[70] Yalcinoz AH, Gursoy Calis GE, Karaca B, et al. Biosynthesis of silver nanoparticles by thermophilic spore-forming bacilli: Screening for high-performance strains and characterization of silver nanoparticles from *Anoxybacillus* sp. D401a. Prep Biochem Biotechnol 2025:1–23. https://doi.org/10.1080/10826068.2025.2532470. PMid: 40680066.
[71] Srimathi R, Sondak T, Kim K. Cell-free supernatant-assisted biogenic silver nanoparticles enhance the antibacterial efficacy of communicating bacterial pathogens. Biotechnol Bioprocess Eng 2024;29(5):902–14. https://doi.org/10.1007/s12257-024-00122-5.
[72] Savvidou MG, Kontari E, Kalantzi S, et al. Green synthesis of silver nanoparticles using the cell-free supernatant of *Haematococcus pluvialis* culture. Materials 2023;17(1):187. https://doi.org/10.3390/ma17010187. PMid: 38204044.
[73] Dolai J, Mandal K, Jana NR. Nanoparticle size effects in biomedical applications. ACS Appl Nano Mater 2021;4(7):6471–96. https://doi.org/10.1021/acsanm.1c00987.
[74] Masarudin MJ, Cutts SM, Evison BJ, et al. Factors determining the stability, size distribution, and cellular accumulation of small, monodisperse chitosan nanoparticles as candidate vectors for anticancer drug delivery: Application to the passive encapsulation of [^{14}C]-doxorubicin. Nanotechnol Sci Appl 2015;8:67–80. https://doi.org/10.2147/NSA.S91785. PMid: 26715842.
[75] Haripriyaa M, Suthindhiran K. Pharmacokinetics of nanoparticles: Current knowledge, future directions and its implications in drug delivery. Future J Pharm Sci 2023;9(1):113. https://doi.org/10.1186/s43094-023-00569-y.
[76] Loo YY, Rukayadi Y, Nor-Khaizura M, et al. *In vitro* antimicrobial activity of green synthesized silver nanoparticles against selected Gram-negative foodborne pathogens. Front Microbiol 2018;9:1555. https://doi.org/10.3389/fmicb.2018.01555. PMid: 30061871.
[77] Bogdanova LR, Valiullina YA, Faizullin DA, et al. Spectroscopic, zeta potential and molecular dynamics studies of the interaction of antimicrobial peptides with model bacterial membrane. Spectrochim Acta A Mol Biomol Spectrosc 2020;242:118785. https://doi.org/10.1016/j.saa.2020.118785. PMid: 32801024.
[78] Menichetti A, Mavridi-Printezi A, Mordini D, et al. Effect of size, shape and surface functionalization on the antibacterial activity of silver nanoparticles. J Funct Biomater 2023;14(5):244. https://doi.org/10.3390/jfb14050244. PMid: 37233354.
[79] Modi SK, Gaur S, Sengupta M, et al. Mechanistic insights into nanoparticle surface–bacterial membrane interactions in overcoming antibiotic resistance. Front Microbiol 2023;14:1135579. https://doi.org/10.3389/fmicb.2023.1135579. PMid: 37152753.